Proceedings of the ASME 2018 International Design Engineering Technical Conferences & Computers and Information in Engineering Conference
IDETC 2018
August 26-29, 2018, Quebec City, Quebec, Canada

DETC2018-86148

OPTIMAL FLOW CONTROL AND SINGLE SPLIT ARCHITECTURE EXPLORATION FOR FLUID-BASED THERMAL MANAGEMENT

Satya R. T. Peddada[1], Daniel R. Herber[1], Herschel C. Pangborn[2], Andrew G. Alleyne[2], and James T. Allison[1]
[1]Department of Industrial and Enterprise Systems Engineering
[2]Department of Mechanical Science and Engineering
University of Illinois at Urbana-Champaign, Urbana, IL 61801
{speddad2, herber1, pangbor2, alleyne, jtalliso}@illinois.edu

ABSTRACT

High-performance cooling is often necessary for thermal management of high power density systems. Both human intuition and vast experience may not be adequate to identify optimal thermal management designs as systems increase in size and complexity. This paper presents a design framework supporting comprehensive exploration of a class of single phase fluid-based cooling architectures. The candidate cooling system architectures are represented using labeled rooted tree graphs. Dynamic models are automatically generated from these trees using a graph-based thermal modeling framework. Optimal performance is determined by solving an appropriate fluid flow control problem, handling temperature constraints in the presence of exogenous heat loads. Rigorous case studies are performed in simulation, with components having variable sets of heat loads and temperature constraints. Results include optimization of thermal endurance for an enumerated set of 4,051 architectures. In addition, cooling system architectures capable of steady-state operation under a given loading are identified.

1 INTRODUCTION

The 21st century is seeing a continuing trend toward greater electrification of systems in industrial, transportation, agricultural, and consumer applications [1–3]. Large quantities of waste thermal energy are generated by high-power electrical systems, including electro-mechanical devices, electronic power converters, battery systems, and other electro-thermal systems. The performance, efficiency, safety, and life cycle of components within these systems can depend strongly on temperature. Therefore, thermal management systems are tasked with maintaining operating temperatures to within their specified limits. While waste thermal energy must ultimately be rejected to the environment, it is often first transferred from heat-generating components to a liquid coolant circulating through a network of pipes. Control of these fluid-based thermal management systems requires determining command inputs to all valves and pumps in the fluid network. Designing and controlling such systems becomes a challenging task as they increase in both size and complexity, commensurate with the systems that they cool.

A thermal management system must not only be energy efficient and reliable, but also help reduce capital cost in terms of cooling network size, complexity, and fabrication cost. Mobile systems have additional considerations, such as weight limitations and more limited options for cooling mechanisms. Cooling system architecture can affect all of the above attributes. Poor architectures can result in sudden failure of heat-sensitive components or lead to long-term degradation when temperature constraints cannot be maintained, while over-cooling can reduce efficiency. The cooling system architecture design must balance maintaining the temperature constraints of individual components with overall system considerations such as pumping efficiency and geometric packaging. System-level needs can vary widely. For example, aircraft thermal management systems need to achieve high thermal endurance, defined as the duration of operation before any temperature constraint is violated, to ensure safe operation and maximum range [4]. Other applications, such as hybrid-electric vehicles [5] or server farms [6] may have a different set of requirements. As new cooling system applications and requirements emerge, engineers must learn how best to meet

new needs, sometimes without the benefit of design heritage or the associated expert knowledge for particular systems. Cooling system architecture design problems can have a vast design space that is cognitively difficult to navigate, motivating efficient systematic design methods with the flexibility to explore and assess new configurations.

Many past efforts have focused on improving individual components in a cooling system, but few have addressed overall system design. Examples of the latter include Refs. [7, 8]. In Ref. [7] a design methodology was developed to predict cooling tower performance considering heat load distributions. In Ref. [8] interactions between a heat-exchanger network and cooling tower were considered. Cooling system architecture studies typically focus on a single application such as process utilities in petrochemical plants [9] or multi-chip processors [10], as opposed to a general design framework. Existing architecture studies have often been limited in scope to improve tractability. For example, rearranging components in a given topology restricts problem complexity, but limits broad exploration of new designs [11].

In this article, simplifying model assumptions are made that support tractability while retaining important physical effects and applicability to a wide range of thermal management system applications. Many of these assumptions have been validated in previous experimental work, and are discussed in more detail in later sections as appropriate. Here we limit the design scope to a fluid-based thermal management system with a single junction and single split. The design methodology presented here:

- Uses dynamic graph-based modeling to provide flexibility in assessing a variety of different cooling system types,
- Supports systems with multiple temperature-sensitive components having high heat loads and different maximum allowable temperatures,
- Is applicable to small to medium-scale systems (extension to large-scale systems is a topic of ongoing work),
- Uses flexible solution methods, such as variable-horizon direct optimal control, to accommodate evaluation of a wide range of system architectures,
- Determines optimal coolant distribution across the system, balancing competing objectives.

Primary contributions include 1) a new method for enumerating system architectures modeled using graphs as labeled rooted trees, and 2) a rigorous method for comparison between candidate architectures. The first contribution builds on recent work in efficient methods for architecture enumeration. The second contribution is enabled by recent advancements in direct optimal control. Flow is distributed optimally across the system such that thermal endurance is maximized across components operating under different heat loads and temperature constraints. The proposed design methodology is applicable to a wide variety of applications. The highest performing architectures are determined as those which maximize the thermal endurance.

The remainder of this article is organized as follows. Section 2 describes the class of thermal management architectures considered in this paper, as well as the graph-based approach used to generate dynamic models of these systems. Section 3 describes how to enumerate architectures as labeled rooted tree graphs for cooling system design. Section 4 explains the variable time horizon dynamic optimization problem formulation. Section 5 presents three case studies performed with different architectures at various sets of operating conditions, heat loads, and individual temperature constraints to demonstrate the efficacy of the design method introduced here. Finally, Section 6 concludes by summarizing the design methodology, outlining guidelines for thermal management system design derived from case study results, and suggests topics for future work.

2 SYSTEM DESCRIPTION AND MODELING

The class of thermal management system architectures considered in this paper is depicted in Fig. 1. The primary purpose of the system is to manage the operating temperature of a number of heat-generating electrical or mechanical components, each mounted to a cold plate heat exchanger (CPHX) through which a coolant flows. This fluid is stored in a tank and driven by a pump through a set of N_f *parallel* flows, each of which includes a variable-aperture valve v. The fluid in each parallel flow passes through a number of CPHXs in *series*, absorbing thermal energy from the CPHX walls. Thermal energy is transferred from the fluid to a thermal sink (e.g., a vapor compression-based chilled loop [12] via a liquid-to-liquid heat exchanger (LLHX). This class of architectures is representative of many single-phase fluid-based thermal management systems, such as those found in aircraft [13, 14], electrified automobiles [15], and server farms [6].

The total number of CPHXs, which is assumed to be fixed for a given design study, is denoted N_c. We also assume that the heat load applied to each CPHX is an exogenous disturbance, and that the temperature of each heat-generating component is the same as the temperature of the wall of the CPHX to which it is mounted. The thermal management system is controlled by commanding the rotational speed of the pump and the position of each variable-aperture valve.

2.1 Dynamic Graph-Based Modeling

One approach for the lumped parameter dynamic modeling of power flow systems, including the class of thermal management architectures considered in this paper, is to apply conservation equations within a graph-based framework, where vertices represent the capacitive storage of energy and edges represent the paths along which power can flow between vertices [12, 16–19]. This graph-based approach is particularly well-suited for architecture exploration and optimization because the models are generated from a structural mapping of interconnections that can be

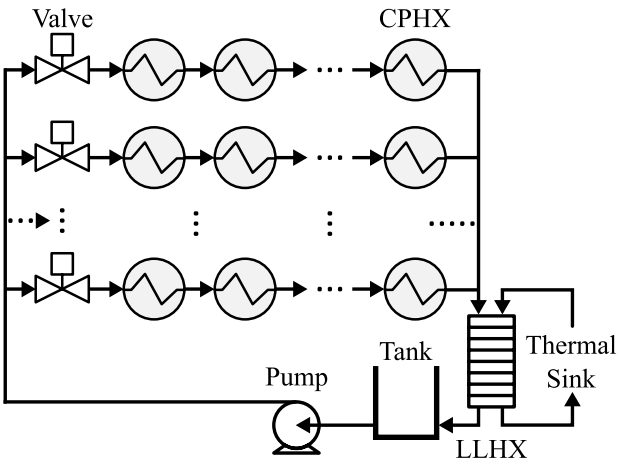

FIGURE 1: Illustration of the class of cooling system architectures considered, consisting of cold plate heat exchangers (CPHXs) in series and parallel, and constrained to have a single split/junction in the coolant flow.

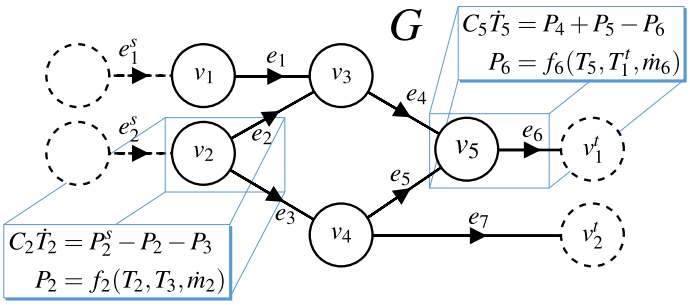

FIGURE 2: Notional graph example to demonstrate key features of the modeling approach.

constructed in a programmatic way and leveraged in both system analysis and control design. The remainder of this subsection presents an overview of the graph-based modeling approach, which is then contextualized to the type of architectures considered in this paper.

In graph-based modeling, the structure of interconnections of the system is described by the oriented graph $G = (\boldsymbol{v}, \boldsymbol{e})$ of order N_v with vertices $\boldsymbol{v} = [v_i], i \in [1, N_v]$, and size N_e with edges $\boldsymbol{e} = [e_j], j \in [1, N_e]$. As shown in the notional graph example of Fig. 2, each edge e_j is incident to two vertices and indicates directionality from its *tail* vertex v_j^{tail} to its *head* vertex v_j^{head}. The set of edges directed into vertex v_i is given by $e_i^{head} = \{e_j | v_j^{head} = v_i\}$, while the set of edges directed out of vertex v_i is given by $e_i^{tail} = \{e_j | v_j^{tail} = v_i\}$ [20].

Each vertex has an associated dynamic state representing energy storage. For thermal systems, this state is the temperature of a thermal element, T_i. Each edge has an associated quantity P_j describing the rate of transfer of thermal energy (equivalently referred to as thermal power flow in this paper) between adjacent vertices. The orientation of each edge indicates the convention assigned to positive power flow, from v_j^{tail} to v_j^{head}. Therefore, the dynamics of each state satisfy the conservation equation:

$$C_i \dot{T}_i = \sum_{\{j | e_j \in e_i^{head}\}} P_j - \sum_{\{j | e_j \in e_i^{tail}\}} P_j \tag{1}$$

where $C_i > 0$ is the thermal capacitance of the vertex. In words, Eqn. (1) states that the rate of thermal energy storage in the vertex is equal to the total thermal power flow into the vertex minus the total thermal power flow out of the vertex.

For the fluid-based thermal system in this paper, the power flow P_j along each edge is a function of the temperature states of the vertices to which it is incident and may also be a function of an associated mass flow rate $\dot{m}_j$ which can be treated as an input to the thermal system model [12, 16–18]. The transfer rate along each edge is therefore given generically by:

$$P_j = f_j\left(T_j^{tail}, T_j^{head}, \dot{m}_j\right) \tag{2}$$

Fig. 2 includes examples of Eqn. (1) and Eqn. (2) as applied to several vertices and edges.

In addition to capturing the exchange of energy within the graph, the modeling framework must account for exchange with entities external to the graph. Sources to graph G are modeled by source edges $\boldsymbol{e}^s = [e_j^s], j \in [1, N_s]$ with associated power flows $\boldsymbol{P}^s = [P_j^s]$, which are treated as disturbances to the system that may come from neighboring systems or the environment. Therefore, edges belonging to $\boldsymbol{e}^s$ are not counted among the edges $\boldsymbol{e}$ of graph G, and transfer rates in $\boldsymbol{P}^s$ are not counted among the internal transfer rates $\boldsymbol{P}$ of the system.

Sinks of graph G are modeled by sink vertices $\boldsymbol{v}^t = [v_j^t], j \in [1, N_t]$ with associated states $\boldsymbol{T}^t = [T_j^t]$. The sink vertices are counted among the vertices $\boldsymbol{v}$ of graph G, but the sink states $\boldsymbol{T}^t$ are not included in the state vector $\boldsymbol{T}$ of the system. Instead, the sink states $\boldsymbol{T}^t$ are treated as disturbances to the system associated with the neighboring systems or environment.

To describe the structure of edge and vertex interconnections of a graph, the incidence matrix $\boldsymbol{M} = [m_{i,j}] \in \mathbb{R}^{N_v \times N_e}$ is defined as:

$$m_{i,j} = \begin{cases} +1 & v_i \text{ is the tail of } e_j, \\ -1 & v_i \text{ is the head of } e_j, \\ 0 & \text{else.} \end{cases} \tag{3}$$

M can then be partitioned as:

$$\boldsymbol{M} = \begin{bmatrix} \bar{\boldsymbol{M}} \\ \underline{\boldsymbol{M}} \end{bmatrix} \text{ with } \bar{\boldsymbol{M}} \in \mathbb{R}^{(N_v - N_t) \times N_e} \tag{4}$$

where the indexing of edges is assumed to be ordered such that $\bar{\boldsymbol{M}}$ is a structural mapping from power flows $\boldsymbol{P}$ to states $\boldsymbol{T}$, and $\underline{\boldsymbol{M}}$ is a structural mapping from $\boldsymbol{P}$ to sink states $\boldsymbol{T}^t$.

Similarly, the connection of external sources to the system

is given by $\boldsymbol{D} = [d_{i,j}] \in \mathbb{R}^{(N_v - N_t) \times N_s}$ where:

$$d_{i,j} = \begin{cases} 1 & v_i \text{ is the head of } e^s_j, \\ 0 & \text{else.} \end{cases} \tag{5}$$

Following from the conservation equation for each vertex in Eqn. (1) and the above definitions of $\bar{\boldsymbol{M}}$ and $\boldsymbol{D}$, the dynamics of all states in a system are given by:

$$\boldsymbol{C}\dot{\boldsymbol{T}} = -\bar{\boldsymbol{M}}\boldsymbol{P} + \boldsymbol{D}\boldsymbol{P}^s \tag{6}$$

where $\boldsymbol{C} = \text{diag}([C_i])$ is the diagonal matrix of capacitances.

Following from Eqn. (2), the vector of all power flows $\boldsymbol{P}$ in a system is given by:

$$\boldsymbol{P} = F(\boldsymbol{T}, \boldsymbol{T}^s, \dot{\boldsymbol{m}}) = [f_j(T^{tail}_j, T^{head}_j, \dot{m}_j)]. \tag{7}$$

2.2 Graph-Based Model for the Class of Architectures

Fig. 3 shows the graph corresponding to the class of system architectures considered in this paper. To model this class using the graph-based approach of Section 2.1, vertices are assigned to represent the temperature of the fluid in the tank, the temperature of the fluid in each CPHX and the wall of each CPHX, and the temperature of the fluid in each side of the LLHX and the wall of the LLHX. The thermal capacitance associated with states representing a fluid temperature in Eqn. (1) is given by $C_i = \rho V_i c_p$, where V is the volume of the stored fluid, c_p is the specific heat capacitance of the fluid, and ρ is the density of the fluid. The thermal capacitance associated with states representing a wall temperature is given by $C_i = M_{w,i} c_{p,w,i}$, where M_w is the mass of the wall and $c_{p,w}$ is the specific heat capacitance of the wall material. All thermal capacitances in this paper are assumed to be constant.

In this paper, the modeling of two types of thermal power flow is required to capture the exchange of thermal energy between temperature states of the graph. The first is power flow due to convective heat transfer, given by $P_j = h_j A_{s,j}(T^{tail}_j - T^{head}_j)$, where A_s is the convective surface area and h is the heat transfer coefficient, assumed to be constant in this paper. This type of power flow occurs between the wall and the fluid of each CPHX, and between the wall and the fluid on each side of the LLHX.

The second type of thermal power flow is advection associated with fluid flow, given by $P_j = \dot{m}_j c_p T^{tail}_j$, where $\dot{m}$ is the mass flow rate of the fluid and c_p is the specific heat capacitance of the fluid, assumed to be constant in this paper. When fluid flows in a loop between two thermal elements, as between the secondary side of the LLHX and the thermal sink, the advective power flow in each direction can be combined into a single "bidirectional advection" power flow, given by $P_j = \dot{m}_j c_p (T^{tail}_j - T^{head}_j)$.

Based on the above discussion, for every power flow in the graph-based model of the class of architectures, Eqn. (2) can be put in the form:

$$P_j = a_{1,j} T^{tail}_j + a_{2,j} T^{head}_j + b_{1,j} \dot{m} T^{tail}_j + b_{2,j} \dot{m} T^{head}_j \tag{8}$$

where the coefficients $a_{i,j}$ and $b_{i,j}$ are constants. The source

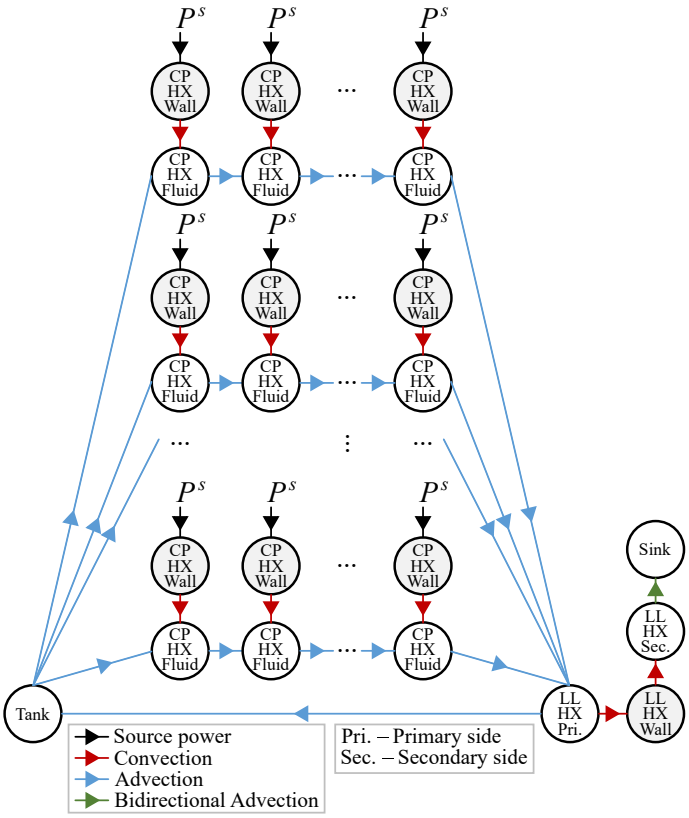

FIGURE 3: Graph for the class of thermal management architectures considered in this paper. Vertices representing fluid temperatures are colored white, while vertices representing wall temperatures are colored gray.

power flows P^s of the graph-based model for the class of system architectures consist of the heat load to each CPHX from the heat-generating device to which it is mounted. The lone sink state of the system T^t is the temperature of the thermal sink.

In this paper, as in Ref. [21], it is assumed that the valves can be controlled such that the flow through the pump can be split with any desired proportioning into each of the parallel flows. It is also assumed that the upper and lower bounds on the mass flow rate achievable by the pump are independent of the number of parallel flows, number of CPHXs in each parallel flow, and valve positions. While the hydraulic modeling that would be necessary to remove this assumption falls outside the scope of this study, previous work has included graph-based modeling of the hydrodynamics of a fluid system, where it is demonstrated that hydraulic and thermal graphs-based models of a system can be interconnected to capture both these domains using a common modeling approach [12, 16].

Experimental validation of the graph-based modeling approach for similar fluid-thermal architectures can be found in [12, 16, 18]. The parameters used in Section 5 were nominally

sized in accordance with the parameters used for experimental validation in that previous work. Several of the key parameters are listed in Table 1. Each CPHX is assumed to be identical, although the heat load applied to each CPHX may be different. The working fluid is assumed to be an equal parts mixture of propylene glycol and water.

2.3 State Equations for the Graph-Based Model

Let $\boldsymbol{M}_a = [\tilde{m}_{i,j}]$ be a weighted incidence matrix defined by:

$$\tilde{m}_{i,j} = \begin{cases} a_{1,j} & \text{if } v_i \text{ is the tail of } e_j, \\ a_{2,j} & \text{if } v_i \text{ is the head of } e_j, \\ 0 & \text{else.} \end{cases} \tag{9}$$

where $a_{i,j}$ are the coefficients in Eqn. (8). $\boldsymbol{M}_b$ can be defined similarly using the coefficients $b_{i,j}$ in Eqn. (8).

Note that there is not a one-to-one relationship between the mass flow rates of the system architecture and the edges of its thermal graph. For example, the mass flow rate through each CPHX of a given parallel flow is the same. Therefore, the set of unique mass flow rates of the system can be mapped to the set of edges of the graph by:

$$\dot{\boldsymbol{m}}_e = \boldsymbol{Z}\begin{bmatrix} \dot{m}_p \\ \dot{\boldsymbol{m}}_f \\ \dot{m}_t \end{bmatrix}, \qquad \boldsymbol{Z} \in \{0,1\}^{N_e \times (2+N_f)} \tag{10}$$

where $\dot{m}_p$ is the mass flow rate rate through the pump, $\dot{\boldsymbol{m}}_f$ is the vector of mass flow rates through each parallel flow, and $\dot{m}_t$ is the mass flow rate of the thermal sink. From Eqn. (6) and Eqns. (8)-(10), the state-space equation for the system architecture can be written as:

$$\dot{\boldsymbol{T}} = \boldsymbol{A}\begin{bmatrix} \boldsymbol{T} \\ T^t \end{bmatrix} + \boldsymbol{B}_1 \text{diag}\left(\boldsymbol{Z}\begin{bmatrix} \dot{m}_p \\ \dot{\boldsymbol{m}}_f \\ \dot{m}_t \end{bmatrix}\right)\boldsymbol{B}_2\begin{bmatrix} \boldsymbol{T} \\ T^t \end{bmatrix} + \boldsymbol{D}\boldsymbol{P}^s \tag{11}$$

where:

$$\boldsymbol{A} = -\boldsymbol{C}^{-1}\bar{\boldsymbol{M}}\bar{\boldsymbol{M}}_a^T \tag{12a}$$

$$\boldsymbol{B}_1 = -\boldsymbol{C}^{-1}\bar{\boldsymbol{M}} \tag{12b}$$

$$\boldsymbol{B}_2 = \bar{\boldsymbol{M}}_b^T \tag{12c}$$

and $\boldsymbol{D}$ is as defined in Eqn. (5). For a given number of parallel flows and number of CPHXs in each flow, the corresponding state-space model in the form of Eqn. (11) can be programmatically generated.

3 GENERATING NEW ARCHITECTURES WITH LABELED ROOTED TREE GRAPHS

3.1 Representation as Labeled Rooted Tree Graphs

The class of architectures $\mathcal{A}$ can be represented as labeled rooted tree graphs. Two example trees are shown in Fig. 4. In graph theory, a tree is a undirected graph in which any two vertices are connected by unique simple path [22, 23]. An equivalent definition is an undirected graph that is connected and has

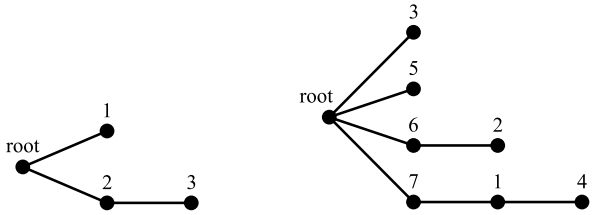

(a) $1-23$. (b) $3-5-62-714$.

FIGURE 4: Two labeled rooted tree graphs in the class of graphs of interest.

no cycles. Here a labeled rooted tree is a tree where the root is labeled with 0 and each other vertex is assigned a unique integer value from 1 to N_c [23]. The architectures in $\mathcal{A}$ are representable by labeled rooted trees because the labels in the tree (other than the root) correspond to specific CPHXs in a predefine list and the fluid is defined to flow away from the root. Finally, to completely define $\mathcal{A}$, we require all the vertices in the tree except the root to have at most one child.

The number of unlabeled rooted trees of interest with $N_c + 1$ nodes is equivalent to the partition numbers (i.e., different ways of writing N_c as a sum of positive integers). For a given partition, each summation represents an additional valve, and the integers represent the number of CPHXs in series with particular v. For example, $1+3+3$ and $1+1+2+3$ are two of the 15 unique partitions for $N_c = 7$. The number of partitions for different N_c is given by OEIS A000041 [23, 24]:

$$S = 1, 2, 3, 5, 7, 11, 15, 22, 30, 42, 56, \ldots \tag{13}$$

However, trees generated using these partitions are unlabeled. To determine the number of labeled rooted trees, we can naively consider all permutations of the vertices for each partition, providing the upper bound on the number of architectures as:

$$|\mathcal{A}(N_c)| \leq N_c! \times S(N_c) \tag{14}$$

This is only an upper bound as there will potentially be isomorphic graphs [23] using the naive permutations. Fortunately, we can directly account for the isomorphic graphs by considering the number of instances of a specific integer in the partition and their permutations:

$$|\mathcal{A}(N_c)| = \sum_{k=1}^{S(N_c)} \left[N_c! \times \left(\prod_{i=1}^{N_c} I(k,i)! \right)^{-1} \right] \tag{15}$$

where $I(k,i)$ is the number of times the integer i appears in partition k (e.g., if we have partition $k: 1+2+2+2$, then $I(k,2) = 3$) and I can be computed with Ref. [25]. The first few values for the number of unique architectures for increasing N_c are 1, 3, 13, 73, 501, 4051, 37633, and 394353. The 13 unique cooling system architectures for $N_c = 3$ are shown in Fig. 5. This information will be used when generating each of the trees.

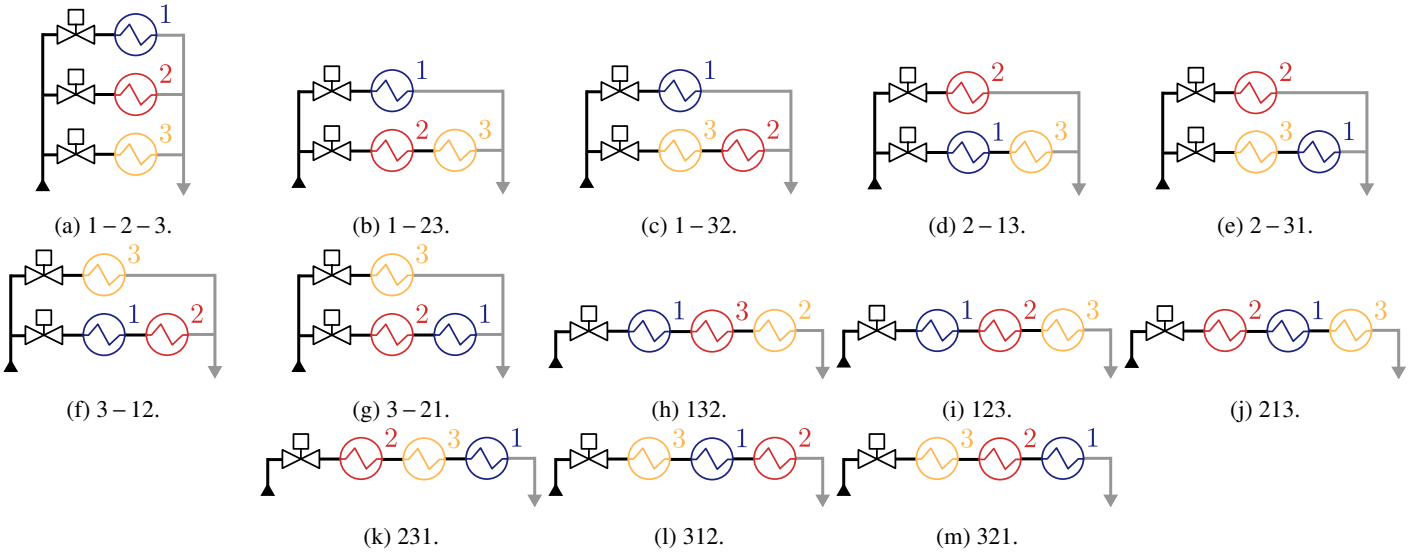

(a) 1 – 2 – 3. (b) 1 – 23. (c) 1 – 32. (d) 2 – 13. (e) 2 – 31.

(f) 3 – 12. (g) 3 – 21. (h) 132. (i) 123. (j) 213.

(k) 231. (l) 312. (m) 321.

FIGURE 5: The 13 unique architectures when $N_c = 3$.

3.2 Generating the Labeled Rooted Tree Graphs

Here we will utilize the parent pointers representation of a tree graph where the k^{th} child (vertex labeled with k) of vector V has the parent node $V(k)$ [22]. For example, $V = [0\ 3\ 0]$ defines the labeled rooted tree in Fig. 5c. To enumerate all possible labeled rooted trees of height two, a recursive algorithm was developed.

Some key features of the approach are:

1. Recursively generating all vectors of length N_c with integer entries from 0 to N_c by adding one child-parent entry at a time.
2. Keeping a list of potential parents and removing vertices that already have a child from this list during the recursion. The root node is always a potential parent. This ensures the single-junction (height two) structure of the trees.
3. Removing any graphs that have a cycle added during the recursion (since they are not trees).

Due to the special structure of the parent pointers representation, all of the generated trees are unique. We can readily generate the listing of all the trees up to $N_c = 10$ where we start to have data storage issues due to the combinatorial nature of the problem. These listings will serve as a basis for evaluating all potential cooling system architectures for a given problem.

4 OPTIMAL FLOW CONTROL PROBLEM

To study the thermal performance of the candidate architectures, a dynamic optimization problem is posed. The goal of this optimization problem is to maximize the thermal endurance of a candidate architecture, defined as the length of time before any temperature state violates its upper bound. This variable time problem therefore provides an upper limit on length of the time horizon t_{end} such that the constraints of the problem are still satisfied:

$$\min_{\dot{\boldsymbol{m}}_f, t_{\text{end}}} \quad -t_{\text{end}} \tag{16}$$

where $\dot{\boldsymbol{m}}_f$ are the open-loop control variables used to regulate the valve flow rates.

The dynamics for this problem are then a combination of Eqn. (11) and additional states to capture $\ddot{\boldsymbol{m}}$:

$$\dot{\boldsymbol{\xi}} = \begin{bmatrix} \dot{\boldsymbol{T}} \\ \ddot{\boldsymbol{m}}_f \end{bmatrix} \tag{17}$$

where $\boldsymbol{T}$ is the vector of temperature states, $\dot{\boldsymbol{T}}$ is given in Eqn. (11), T^t is the temperature of the thermal sink (the chiller), and there are $n_\xi = 4 + 2N_c + N_f$ states.

The next constraint initializes the temperature states of the system:

$$\boldsymbol{T}_w(0) = T_{w,0}, \quad \boldsymbol{T}_f(0) = T_{f,0}, \quad \boldsymbol{T}_l(0) = T_{l,0} \tag{18}$$

where $T_{w,0}$ is the initial temperature of the cold plate walls, $T_{f,0}$ is the initial temperature of the cold plate fluids, and $T_{l,0}$ is the initial temperature of the tank and LLHX states.

To ensure that each component remains within an upper bound on its operating temperature, we include the following linear inequality path constraints on the temperature states:

$$\boldsymbol{T}_w(t) \le \boldsymbol{T}_{w,\max}, \quad \boldsymbol{T}_f(t) \le \boldsymbol{T}_{f,\max}, \quad \boldsymbol{T}_l(t) \le \boldsymbol{T}_{l,\max} \tag{19}$$

where $\boldsymbol{T}_{w,\max} \in \mathbb{R}^{N_c}$ are the maximum allowable temperatures for the CPHX walls, $\boldsymbol{T}_{f,\max} \in \mathbb{R}^{N_c}$ are the maximum allowable temperatures for the CPHX fluids, and $\boldsymbol{T}_{l,\max} \in \mathbb{R}^4$ are the maximum allowable temperatures for the tank and LLHX states.

We also ensure nonnegative flow through each of the valves

(i.e, no fluid flow in the reverse direction) with the following linear inequality path constraint:

$$0 \leq \dot{\boldsymbol{m}}_f \tag{20}$$

A static form of conservation of mass ensures that the total mass flow rate through all the parallel flows is equal to the mass flow rate through the pump with the following linear equality path constraint:

$$\sum_{i=1}^{N_f} \dot{m}_{f,i}(t) = \dot{m}_{\text{pump}} \tag{21}$$

where $\dot{m}_{\text{pump}}$ is the constant flow rate of the pump.

To model a limit on the rate of change of the valve positions, we also enforce constraints on the derivative of the mass flow rates:

$$|\ddot{\boldsymbol{m}}_f(t)| \leq \ddot{m}_{f,\max} \tag{22}$$

where $\ddot{m}_{f,\max}$ is the maximum allowable value.

Finally, we impose a small quadratic penalty term on the controls to both smooth the solution trajectories and improve convergence, modifying Eqn. (16) to:

$$\min_{\ddot{\boldsymbol{m}}, t_{\text{end}}} \quad -t_{\text{end}} + \lambda \int_0^{t_{\text{end}}} \|\ddot{\boldsymbol{m}}_f(t)\|_2^2 dt \tag{23}$$

where λ is the penalty parameter and is chosen such that $\lambda \ll 1/(N_f \ddot{m}_{f,\max}^2)$ (i.e., there is a limited overall effect on the objective function value).

For the pure series architectures ($N_f = 1$), we developed a simple shooting-based, bisection method that quickly determines the optimal value of t_{end} assuming the maximum allowable flow rate.

5 CASE STUDIES

Here we present several case studies to demonstrate both the efficacy and utility of the design methodology for cooling system architectures. The nonlinear optimal control problem presented in Section 4 was solved using GPOPS-II, which discretizes the problem using pseudospectral methods into a finite-dimensional nonlinear program [26]. The key model and optimization problem parameters used in the case studies are given in Table 1.

5.1 Case Study 1

Here we study cooling system architectures that have three CPHXs. As shown in Fig. 5 and Section 3, there are thirteen unique architectures possible. For these results, we assume that all temperature constraints are equal to 45 °C and that the total heat load on the cooling system is equal to 15 kW.

5.1.1 Identical Heat Loads

The first set of results has an identical heat load to each CPHX, resulting in only three unique architectures. The results are shown in Fig. 6. The optimal values for t_{end} were $(133, 129, 123)$ s, for the (pure parallel, hybrid, pure series) architectures, respectively. This result indicates that the commonly used pure parallel architecture is in fact the best one under these conditions. Note that in each of the cases, at least one of the temperature constraints is active at the final time (a necessary stopping condition), and for both $1-2-3$ and $1-32$, all the wall temperatures are at their maximum allowable value.

TABLE 1: Key model and optimization problem parameters.

Parameter	Value
CPHX wall mass	1.15 kg
LLHX wall mass	1.2 kg
Tank fluid mass	2.01 kg
Thermal sink temperature T^t	15 °C
Tank/LLHX initial temperatures, $T_{l,0}$	15 °C
CPHX initial wall temperatures, $T_{w,0}$	20 °C
CPHX initial fluid temperatures, $T_{f,0}$	20 °C
Thermal sink mass flow rate, $\dot{m}_t$	0.2 kg/s
Pump mass flow rate, $\dot{m}_p$	0.4 kg/s
Valve rate limit, $\ddot{m}_{f,\max}$	0.05 kg/s^2
Penalty parameter, λ	5×10^{-3}

5.1.2 Unique Heat Loads

The next set of results, shown in Fig. 7, have a unique and linearly spaced heat load to each CPHX. Here the best architecture is a series topology, 321, with $t_{\text{end}} = 234$ s (in fact, there would only be a minor constraint violation of 0.25 °C were the constraint softened such that the system could reach steady-state). The pure parallel architecture was 7th best overall with $t_{\text{end}} = 119$ s. The worst result was found to be 123, with $t_{\text{end}} = 71$ s. It is observed that the CPHX with the highest heat load (3) should always be connected to the root to achieve good thermal endurance. In addition, many of the solutions have some of the temperature path constraints active for long periods of time (up to 80 s).

5.1.3 Grouped Heat Loads

Here we consider the case when two CPHXs have the same heat load and the third is double the heat load of the first two. The results are shown in Fig. 8. Again, the series 321 and 312 (identical models) performed the best with $t_{\text{end}} = 199$ s and the pure parallel was 5th with $t_{\text{end}} = 119$ s. Comparing these results to unique heat loads, we see that the best architecture performs worse with these grouped heat loads than in the unique case, even though the total heat load on the system is the same.

5.2 Case Study 2

Unlike in case study 1, here we select arbitrary values for both the temperature constraints and heat loads; thus, it is quite challenging to determine through intuition the optimal architecture.

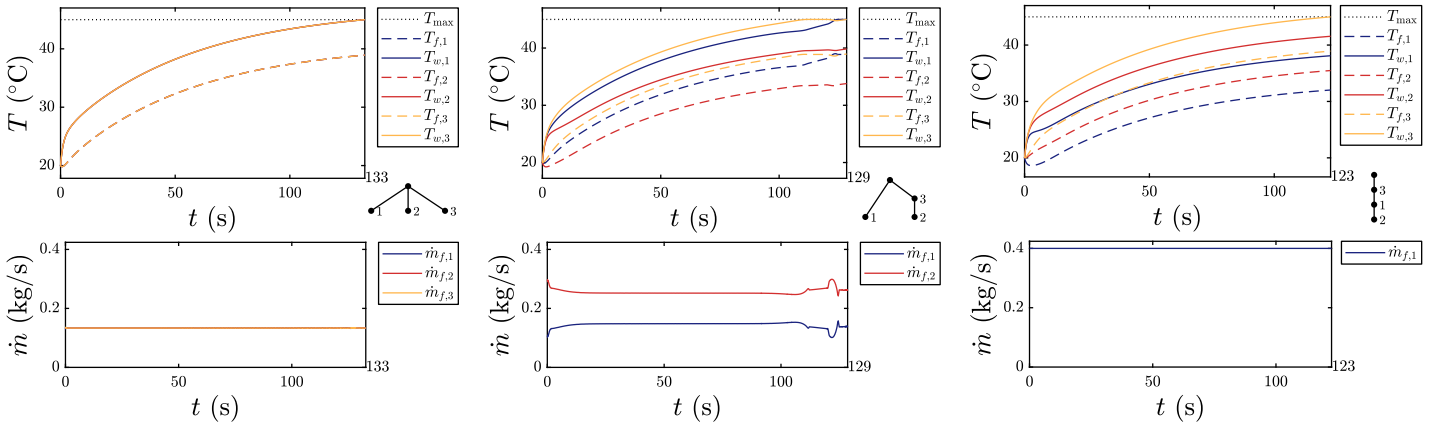

(a) Best architecture with $N_f = 3$ (1 – 2 – 3). (b) Best architecture with $N_f = 2$ (1 – 32). (c) Best architecture with $N_f = 1$ (312).

FIGURE 6: Optimal temperature and flow trajectories for the best architectures with $\boldsymbol{P}^s = [5,5,5]'$ kW and $T_{\max} = 45$ °C.

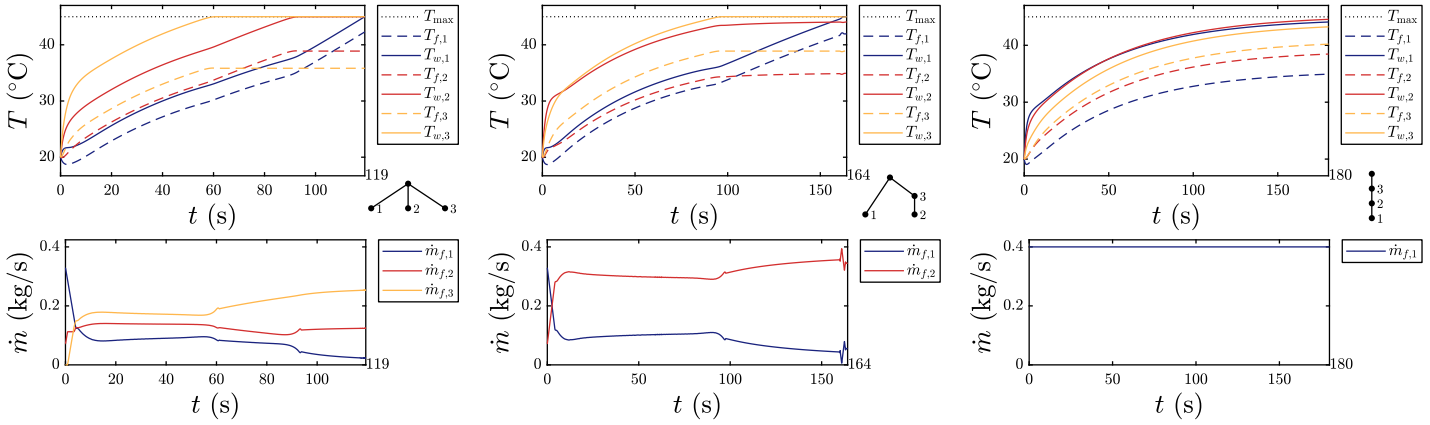

(a) Best architecture with $N_f = 3$ (1 – 2 – 3). (b) Best architecture with $N_f = 2$ (1 – 32). (c) Best architecture with $N_f = 1$ (321).

FIGURE 7: Optimal temperature and flow trajectories for the best architectures with $\boldsymbol{P}^s = [2.5,5,7.5]'$ kW and $T_{\max} = 45$ °C.

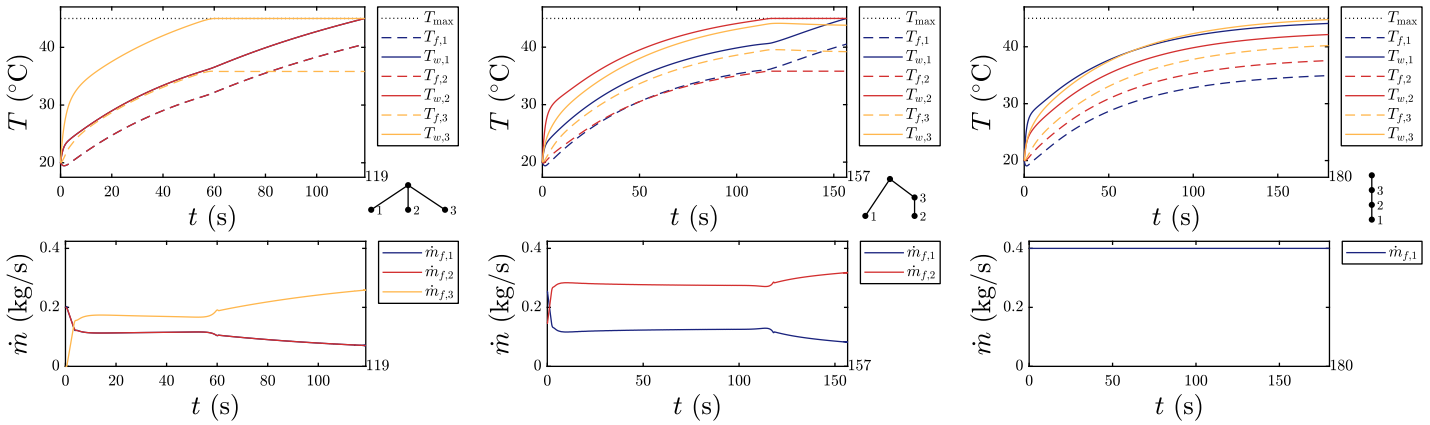

(a) Best architecture with $N_f = 3$ (1 – 2 – 3). (b) Best architecture with $N_f = 2$ (1 – 32). (c) Best architecture with $N_f = 1$ (321).

FIGURE 8: Optimal temperature and flow trajectories for the best architectures with $\boldsymbol{P}^s = [3.75,3.75,7.5]'$ kW and $T_{\max} = 45$ °C.

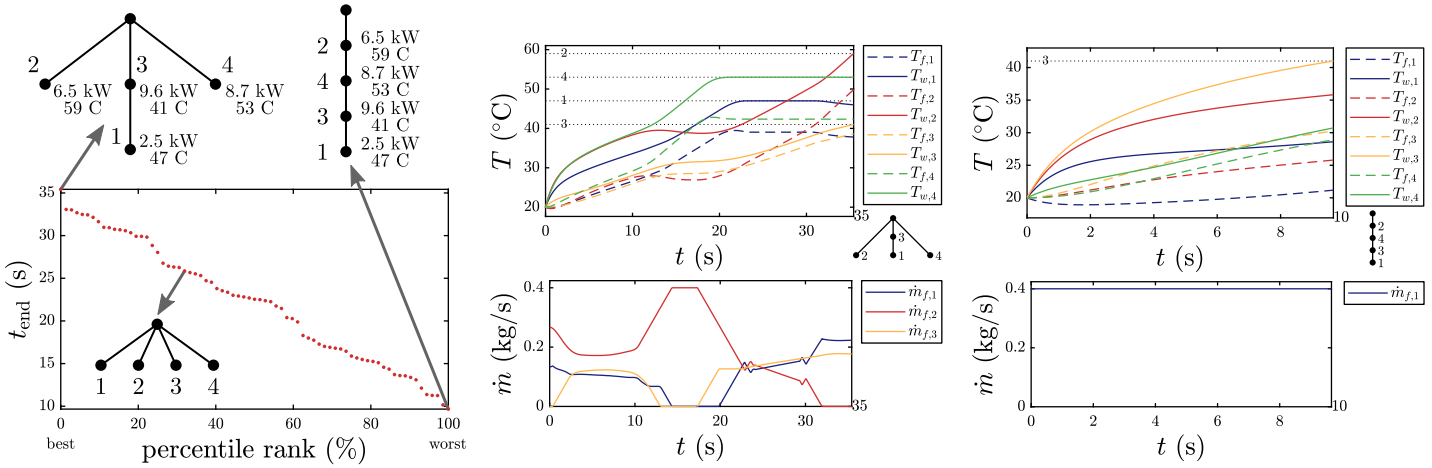

(a) Sorted results for all 73 architectures. (b) Best architecture (2 – 4 – 31). (c) Worst architecture (2431).

FIGURE 9: Results from case study 2 for enumeration with four CPHXs.

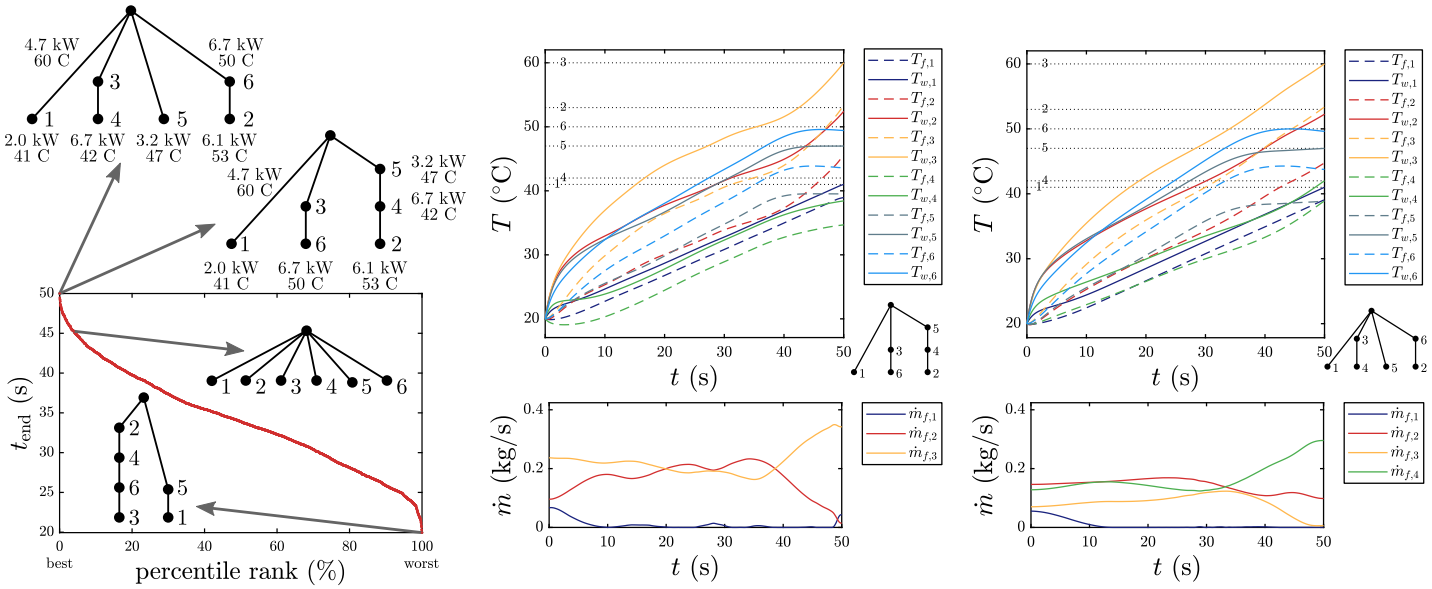

(a) Sorted results for all 4051 architectures. (b) Best with $N_f = 3$ (1 – 36 – 542). (c) Best with $N_f = 4$ (1 – 5 – 34 – 62).

FIGURE 10: Results from case study 2 for enumeration with six CPHXs.

5.2.1 Enumeration with Four CPHXs

For this first result, we consider a problem with four CPHXs and:

$$\boldsymbol{P}^s = [2.5, 6.5, 9.6, 8.7]' \text{ kW}, \quad \boldsymbol{T}_{w,\max} = [47, 59, 41, 53]' \text{ °C}$$

The results for all 73 architectures is summarized in Fig. 9a.The best architecture was 2 – 4 – 31.This differs from the previous case study, where either pure series or pure parallel was determined to be the best. Observing the trajectories in Fig. 9b shows a large amount of constraint activity.The pure parallel architecture was the 20th best architecture and had a much shorter thermal endurance than the best (27 s vs. 35 s).

5.2.2 Enumeration with Six CPHXs

This study is structured similarly to the previous result but with six CPHXs:

$$\boldsymbol{P}^s = [2.0, 6.1, 4.7, 6.7, 3.2, 6.7]' \text{ kW}$$

$$\boldsymbol{T}_{w,\max} = [41, 53, 60, 42, 47, 50]' \text{ °C}$$

The results for all 4051 architectures are summarized in Fig. 10a.

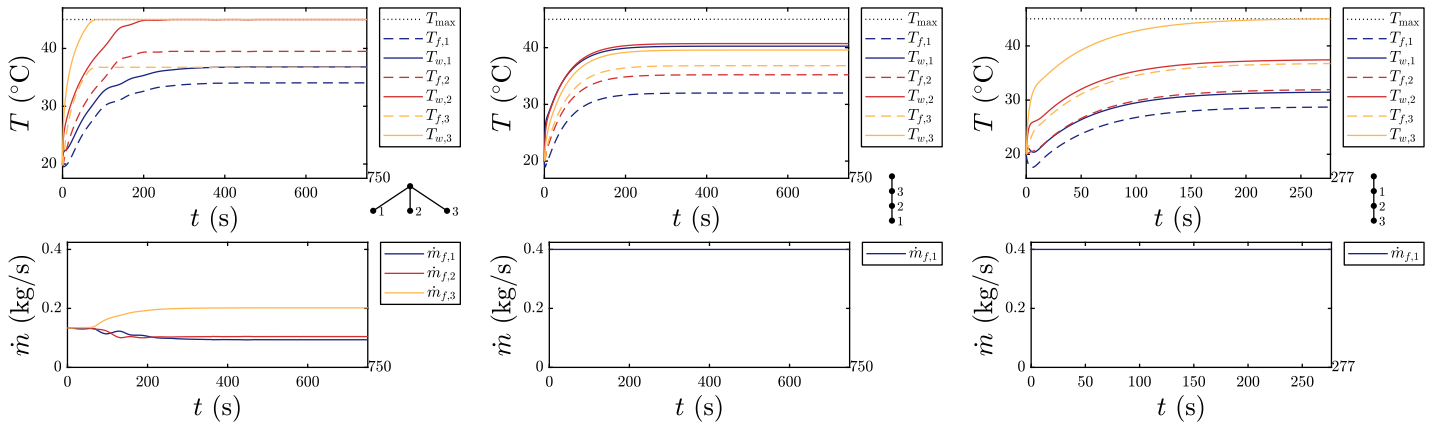

(a) Feasible architecture with $N_f = 3$ (1 – 2 – 3). (b) Feasible architecture with $N_f = 1$ (321). (c) Infeasible architecture with least t_{end} (123).

FIGURE 11: Select results for $\boldsymbol{P}^s = [2.25, 4.5, 6.75]$ kW and $T_{\max} = 45$ °C with steady-state solutions.

Here two architectures had equivalent maximum thermal endurance of 50 s, namely 1 – 36 – 542 and 1 – 4 – 34 – 62. The architecture 1 – 36 – 542 might be preferred since it has a fewer number of flows to control. The temperature and flow rate trajectories for both of these architectures are shown in Figs. 10b and 10c. As with the previous result, the solution is not necessarily intuitive. Additionally, since we evaluated all 4051 architectures, we have a large amount of information to aid in choosing the architecture that is the best for the requirements in this case study. For example, patterns with desirable properties can be observed for the problem of interest, which is beyond what is possible when only generating a *single* optimal design.

5.3 Case Study 3

In the final case study, we consider the goal of determining whether a feasible steady-state operating condition can be reached for a given set of heat loads and temperature constraints. To test this property, we set an upper bound on t_{end} of 1000 s as a conservative estimate of the maximum duration that a feasible architecture could take to reach state-state. Here we used unique and linearly spaced heat loads with $N_c = 3$, similar to Section 5.1.2 except now with a slightly reduced total heat load of 13.5 kW. The results for several of the architectures are shown in Fig. 11. Of the 13 candidates, 11 were able to handle the heat loads for 1000 s. The two that were unable to satisfy the conditions were 123 and 213. The remaining candidates with feasible steady-state solutions are distinguished by differing numbers of CPHXs hitting their upper temperature bound. Architecture 321 in Fig. 11b had the lowest maximum temperature of 41 °C, so none of the constraints were active. These results demonstrate the sensitivity with respect to the total heat load, as many architectures with 13.5 kW total heat load can operate indefinitely, while the best architecture with 15 kW could only last 234 s.

6 CONCLUSION

This work serves as a preliminary study toward design of novel fluid-based thermal management architectures with optimal coolant flow control. Candidate cooling system design architectures have been generated using labeled trees and a graph-based dynamic thermal modeling framework. A variable horizon optimal control problem was posed to identify cooling architectures having maximum thermal endurance. The optimal solutions obtained show that intuition and experience may not be sufficient to identify the best-performing cooling architectures, especially as complexity increases. Three case studies were performed that demonstrated the effectiveness and potential of the proposed design methodology. In particular, this methodology serves as an efficient tool to find both feasible and infeasible architectures at different operating conditions. Future work will incorporate the hydraulic graph-based models of Refs. [12, 16] in the optimization problem to capture the pressure drops and resulting mass flow rate constraints associated with each candidate architecture of the cooling system. In addition, future work will explore a fixed-horizon optimization problem in which the objective is to minimize violations of soft upper bounds on component temperatures over the duration of a representative time varying load profile, similar to that used for control in Ref. [12]. Lastly, future work will leverage the modularity of the graph-based modeling approach to explore architectures with more degrees of freedom in the component topology.

ACKNOWLEDGMENT

This material is based upon work supported by the National Science Foundation Engineering Research Center (NSF ERC) for Power Optimization of Electro-Thermal Systems (POETS) with cooperative agreement EEC-1449548, and the National Science Foundation Graduate Research Fellowship under Grant Number DGE-1144245.

REFERENCES

[1] Kassakian, J. G., and Jahns, T. M., 2013. "Evolving and emerging applications of power electronics in systems". *IEEE Journal of Emerging and Selected Topics in Power Electronics,* ***1***(2), June, pp. 47–58. doi: 10.1109/JESTPE.2013.2271111

[2] Lequesne, B., 2015. "Automotive electrification: The nonhybrid story". *IEEE Transactions on Transportation Electrification,* ***1***(1), June, pp. 40–53. doi: 10.1109/TTE.2015.2426573

[3] Yu, X. E., Xue, Y., Sirouspour, S., and Emadi, A., 2012. "Microgrid and transportation electrification: A review". In IEEE Transportation Electrification Conference and Expo, pp. 1–6. doi: 10.1109/ITEC.2012.6243464

[4] Doman, D. B., 2016. "Fuel flow control for extending aircraft thermal endurance part II: Closed loop control". In AIAA Guidance, Navigation, and Control Conference. doi: 10.2514/6.2016-1621

[5] Park, S., and Jung, D., 2010. "Design of vehicle cooling system architecture for a heavy duty series-hybrid electric vehicle using numerical system simulations". *Journal of Engineering for Gas Turbines and Power,* ***132***(9), Sept., p. 092802. doi: 10.1115/1.4000587

[6] Ouchi, M., Abe, Y., Fukagaya, M., Ohta, H., Shinmoto, Y., Sato, M., and Iimura, K.-i., 2012. "Thermal management systems for data centers with liquid cooling technique of CPU". In IEEE Intersociety Conference on Thermal and Thermomechanical Phenomena in Electronic Systems, pp. 790–798. doi: 10.1109/ITHERM.2012.6231507

[7] Kim, J.-K., and Smith, R., 2001. "Cooling water system design". *Chemical Engineering Science,* ***56***(12), June, pp. 3641–3658. doi: 10.1016/S0009-2509(01)00091-4

[8] Panjeshahi, M. H., Ataei, A., Gharaie, M., and Parand, R., 2009. "Optimum design of cooling water systems for energy and water conservation". *Chemical Engineering Research and Design,* ***87***(2), Feb., pp. 200–209. doi: 10.1016/j.cherd.2008.08.004

[9] Muller, C. J., and Craig, I. K., 2016. "Energy reduction for a dual circuit cooling water system using advanced regulatory control". *Applied Energy,* ***171***, June, pp. 287–295. doi: 10.1016/j.apenergy.2016.03.069

[10] Delia, D. J., Gilgert, T. C., Graham, N. H., Hwang, U., Ing, P. W., Kan, J. C., Kemink, R. G., Maling, G. C., Martin, R. F., Moran, K. P., Reyes, J. R., Schmidt, R. R., and Steinbrecher, R. A., 1992. "System cooling design for the water-cooled IBM enterprise system/9000 processors". *IBM Journal of Research and Development,* ***36***(4), July, pp. 791–803. doi: 10.1147/rd.364.0791

[11] Kim, J.-K., Lee, G. C., Zhu, F. X. X., and Smith, R., 2002. "Cooling system design". *Heat Transfer Engineering,* ***23***(6), pp. 49–61. doi: 10.1080/01457630290098754

[12] Pangborn, H. C., Koeln, J. P., Williams, M. A., and Alleyne, A. G., 2018. "Experimental validation of graph-based hierarchical control for thermal management". *Journal of Dynamic Systems, Measurement, and Control,* ***140***(10), Oct., p. 101016. doi: 10.1115/1.4040211

[13] McCarthy, K., Walters, E., Heltzel, A., Elangovan, R., Roe, G., Vannice, W., Schemm, C., Dalton, J., Iden, S., Lamm, P., Miller, C., and Susainathan, A., 2008. "Dynamic thermal management system modeling of a more electric aircraft". In Power Systems Conference, no. Paper no. 2008-01-2886. doi: 10.4271/2008-01-2886

[14] Ganev, E., and Koerner, M., 2013. "Power and thermal management for future aircraft". In AeroTech Congress & Exhibition, no. 2013-01-2273. doi: 10.4271/2013-01-2273

[15] Kim, E., Shin, K. G., and Lee, J., 2014. "Real-time battery thermal management for electric vehicles". In ACM/IEEE International Conference on Cyber-Physical Systems, pp. 72–83. doi: 10.1109/ICCPS.2014.6843712

[16] Koeln, J. P., Williams, M. A., Pangborn, H. C., and Alleyne, A. G., 2016. "Experimental validation of graph-based modeling for thermal fluid power flow systems". In ASME Dynamic Systems and Control Conference, no. DSCC2016-9782, p. V002T21A008. doi: 10.1115/DSCC2016-9782

[17] Moore, K. L., Vincent, T. L., Lashhab, F., and Liu, C., 2011. "Dynamic consensus networks with application to the analysis of building thermal processes". *IFAC Proceedings Volumes,* ***44***(1), Jan., pp. 3078–3083. doi: 10.3182/20110828-6-IT-1002.02549

[18] Williams, M. A., Koeln, J. P., Pangborn, H. C., and Alleyne, A. G., 2018. "Dynamical graph models of aircraft electrical, thermal, and turbomachinery components". *Journal of Dynamic Systems, Measurement, and Control,* ***140***(4), Apr., p. 041013. doi: 10.1115/1.4038341

[19] Preisig, H. A., 2009. "A graph-theory-based approach to the analysis of large-scale plants". *Computers & Chemical Engineering,* ***33***(3), Mar., pp. 598–604. doi: 10.1016/j.compchemeng.2008.10.016

[20] West, D. B., 2001. *Introduction to Graph Theory*, 2nd ed. Pearson.

[21] Doman, D. B., 2017. "Fuel flow control for extending aircraft thermal endurance". *Journal of Thermophysics and Heat Transfer,* ***32***(1), Jan., pp. 35–50. doi: 10.2514/1.T5142

[22] Cormen, T. H., Leiserson, C. E., Rivest, R. L., and Stein, C., 2009. *Introduction to Algorithms*, 3rd ed. MIT Press.

[23] Riordan, J., 1960. "The enumeration of trees by height and diameter". *IBM Journal of Research and Development,* ***4***(5), Nov., pp. 473–478. doi: 10.1147/rd.45.0473

[24] A000041. The on-line encyclopedia of integer sequences. url: https://oeis.org/A000041

[25] D'Errico, J., 2008. Partitions of an integer. MATLAB File Exchange. url: https://www.mathworks.com/matlabcentral/fileexchange/12009

[26] Patterson, M. A., and Rao, A. V., 2014. "GPOPS-II: a matlab software for solving multiple-phase optimal control problems using hp-adaptive gaussian quadrature collocation methods and sparse nonlinear programming". *ACM Transactions on Mathematical Software,* ***41***(1), Oct. doi: 10.1145/2558904